Dalton Transactions

Accepted Manuscript

ROYAL SOCIETY OF CHEMISTRY

www.rsc.org/dalton

One-pot synthesis of PEG modified $BaLuF_5$: Gd/Yb/Er nanoprobes for dual-modal *in vivo* upconversion luminescent and X-ray bioimaging

Ling Rao,[a,b] Wei Lu,[c] Tianmei Zeng,[a] Zhigao Yi, [a,b] Haibo Wang,[a,b] Hongrong Liu[a] and Songjun Zeng[*a]

Received (in XXX, XXX) Xth XXXXXXXXX 20XX, Accepted Xth XXXXXXXXX 20XX
DOI: 10.1039/b000000x

Polyethylene glycol (PEG) modified $BaLuF_5$:Gd/Yb/Er upconversion nanoparticles (UCNPs) were synthesized by a facile one-pot hydrothermal method for simultaneous synthesis and surface functionalization. The novel, excellently biocompatible and water-soluble bioprobes were used for simultaneous upconversion (UC) luminescence and X-ray bioimaging for the first time. The as-prepared $BaLuF_5$:Gd/Yb/Er UCNPs possess an face-centered cubic structure with an average size of 23.7±2.7 nm. Under 980 nm laser excitation, these UCNPs emitted intense UC luminescence via two-photon process. *In vitro* bioimaging and localized luminescent spectra detected from HeLa cells and background reveal that these UCNPs are ideal candidates for optical bioimaging with absence of autofluorescence. Furthermore, the synergistic *in vivo* UC luminescent and X-ray bioimaging reveal that these PEG-modified $BaLuF_5$:Gd/Yb/Er UCNPs can be successfully used as ideal dual-modal bioprobes. These results demonstrate that these PEG modified UCNPs are ideal multi-modal nanoprobes for bioimaging.

1. Introduction

During the past decades, rare earth compounds have evoked much attention due to their unique 4*f* electronic structure which can absorb and emit various wavelength of electromagnetic radiation from ultraviolet, visible light to near infrared, therefore, the rare earth luminescent materials possess abundant fluorescence characteristics.[1-13] These special characteristics have potential applications in many fields, such as near-infrared quantum counter phosphors, lasers, solar cells, three-dimensional display, sensors, bioimaging as well as clinical therapy.[14-25] Among all the UC nanomaterials, lanthanide (Ln^{3+}) doped rare earth fluorides have been always studied extensively for their low phonon energy, which decreases the probability of the non-radiative relaxation and is beneficial for increasing UC efficiency.[26-28] UCNPs with weak auto-fluorescence used as probes for bioimaging can not only improve the detection sensitivity and signal-to-noise ratio but also can penetrate into the deeper tissue.[29-35] Most reports have been focused on the development of Ln^{3+} doped $NaLnF_4$ UCNPs for luminescent bioimaging.[36-43] As an important kind of host materials, $BaLnF_5$ UCNPs have not been paid so much attention.[44,45] Apart from the excellent UC property, $BaLnF_5$ can also be used as X-ray bioimaging contrast agent because of the large K-edge values ($Ba_{K\text{-}edge}$: 37.4 keV) and high X-ray mass absorption coefficient of Ba element (60 keV, Ba: 8.51 $cm^2\ g^{-1}$).[46] In addition, the recent researches reveal the heavy elements with high atomic number (Z=58-66) can be used as ideal contrast agent. [47-49] Therefore, $BaLnF_5$ can be an ideal dual-modal bioprobe for UC and X-ray bioimaging. In addition, except the Ba^{2+}, some Ln^{3+} also have excellent X-ray absorption property, such as Lu^{3+}, Gd^{3+}, and Yb^{3+}. The K-edge values of Gd^{3+} and Yb^{3+} are 50.2 and 61 keV. And the X-ray mass absorption coefficients of Gd^{3+} and Yb^{3+} are 3.15 and 9.37 $cm^2\ g^{-1}$ at the voltage of 60 keV, while 6.91 and 7.25 $cm^2\ g^{-1}$ at the voltage of 80 keV, respectively. On the other hand, Lu^{3+} also possess large K-edge values ($Lu_{K\text{-}edg}$: 63 keV) and high X-ray mass absorption coefficients (60 keV, Lu: 4.15 $cm^2\ g^{-1}$; at 80 keV, Lu: 7.16 $cm^2\ g^{-1}$),[46] indicating $BaLuF_5$ UCNPs can be used as ideal dual-modal bioprobes for UC fluorescence and X-ray bioimaging. So, combining the Ba^{2+} and Lu^{3+}, Gd^{3+} or Yb^{3+}, the $BaLnF_5$ UCNPs can be an ideal contrast agent from low to high voltage, indicating the sample can be used for various tissue and different age of people. So far, Lu has demonstrated the excellent properties of $BaYbF_5$@SiO_2@PEG as contrast agent in *in vivo* X-ray computed tomography (CT).[50] Our group developed $BaYF_5$:Yb/Er UCNPs for UC fluorescence and *in vivo* CT imaging by simultaneous synthesis and amine-functionalization.[51] $BaGdF_5$ UCNPs as ideal bioprobes were also widely used in UC luminescence, X-ray bioimaging and magnetic resonance imaging (MRI).[33,52,53] Recently, Mahalingam's group reported the synthesis and inter-particle energy transfer of the sub-10 nm lanthanide doped $BaLuF_5$ UCNPs synthesized by a thermal-decomposition method.[54] However, the hydrophobic $BaLuF_5$ UCNPs prepared by thermal-decomposition method need further surface modification for converting to hydrophilic UCNPs, which will limit their applications in bioimaging. Although $BaLuF_5$ UCNPs possess excellent UC and X-ray absorption properties, there is still no report on the simultaneous synthesis/surface modification and multi-modal bioimaging of the hydrophilic PEG-modified $BaLuF_5$ UCNPs.

Herein, Gd^{3+}, Yb^{3+} and Er^{3+} (30%/20%/2%) co-doped $BaLuF_5$ UCNPs were synthesized by a simple one-step method of simultaneous synthesis and surface modification with PEG. The structure, morphology and UC properties of the as-prepared samples were discussed. Furthermore, the *in vitro* HeLa cell bioimaging and dual-modal *in vivo* fluorescence/X-ray bioimaging of $BaLuF_5$ UCNPs were studied in detail for the first time.

2. Experimental

2.1 Chemicals and materials

Polyethyleneglycol (PEG, average molecular = 5000), $Ln(NO_3)_3{\cdot}6H_2O$ (Ln = Lu, Yb, Er and Gd), $BaCl_2$ (99.99%), NH_4F and ethanol were all purchased from Sinopharm Chemical Reagent Co., China. All of these chemical reagents were used as received without any further purification.

2.2 One-pot synthesis of PEG-modified $BaLuF_5$:Gd/Yb/Er UCNPs

The PEG-modified $BaLuF_5$:Gd/Yb/Er UCNPs were synthesized by a modified one-pot hydrothermal method.[33] Firstly, 1.0 g of PEG was added into 20 mL of deionized water containing 1 mL of $BaCl_2$ (1 M) and the mixture was stirred vigorously for 10 minutes. Then, a total amount of 1 mmol of $Ln(NO_3)_3$ (Ln = Lu, Yb, Er and Gd ,0.5 M) with the proportion of 48:30:20:2 were added into the above mixture solution under vigorously stirring. Finally 6 mL of NH_4F (1 M) was added. The obtained mixture solution was agitated for another 10 minutes and then transferred into a 50 mL stainless Teflon-lined autoclave and kept at 190 ℃ for 24 h. After reacting completely, the system was cooled down to room temperature naturally. The prepared samples were washed several times with ethanol and de-ionized water to remove other residual solvents by centrifugation, and then dried in a vacuum drying oven at 60 ℃ for 24 h. The $BaLuF_5$ UCNPs without doping Gd^{3+} were also prepared by the above procedure.

2.3 Characterization

The crystal phase of the as-prepared $BaLuF_5$:Gd/Yb/Er UCNPs were detected by powder X-ray diffraction (XRD) using a Rigaku D/max 2500 System X-ray diffractometer with a scanning rate of $0.02^o{\cdot}s^{-1}$ in the 2θ range from 20^o to 80^o. The morphology and size of these nanocrystals were characterized via a transmission electron microscope (TEM, JEOL-2100F) with an acceleration voltage of 200 kV. Under 980 nm excitation, the UC emission spectra were recorded.

2.4 *In vitro* cell imaging

HeLa cells were grown in Dulbecco's Modified Eagle's Medium supplemented with the hydrophilic $BaLuF_5$:Gd/Yb/Er UCNPs (100 μg/mL), 10% fetal bovine serum and 1% penicilin and streptomycin at 37 ℃ and 5% CO_2. After 4 h, the residual UCNPs were washed several times with phosphate buffer solution (PBS). Then HeLa cells incubated with these UCNPs were imaged by a commercial confocal laser scanning microscope (ZEISS LSM-710 NLO) with 980 nm excitation. The green and red channels were recorded at the spectral regions of 500-600 and 600-700 nm, respectively.

2.5 *In vivo* X-ray bioimaging

A nude mouse was intraperitoneally injected with 10 wt% chloral hydrate solution. And then 200 μL of the PEG-modified $BaLuF_5$ aqueous solution (3 $mg{\cdot}mL^{-1}$) was subcutaneously injected into the mouse. After the injection, the X-ray imaging was detected by a multi-modal *in vivo* imaging system (Bruker *In Vivo* FX PRO) with X-ray imaging functionality. The X-ray bioimagings were recorded with the exposure time of 30 s at 45 kV.

2.6 *In vivo* UC and X-ray imaging

To study the *in vivo* UC/X-ray dual-modal imaging, 10 wt% chloral hydrate solution was intraperitoneally injected into a nude mouse firstly, then 200 μL of the PEG-modified $BaLuF_5$ aqueous solution with the concentration of 3 $mg{\cdot}mL^{-1}$ was subcutaneously injected. After the injection, the UC/X-ray dual-modal imaging was carried out by a multi-modal *in vivo* imaging system (Bruker *In Vivo* FX PRO) with an external 980 nm laser as the excitation source and X-ray imaging functionality. The UC fluorescence and X-ray bioimagings were recorded with the exposure time of 30 s.

3. Results and discussions

3.1 Structure Characterization of $BaLuF_5$:Gd/Yb/Er UCNPs

The water-soluble $BaLuF_5$ UCNPs doped with 30% Gd^{3+}, 20% Yb^{3+} and 2% Er^{3+} were synthesized by a facile one-pot hydrothermal method using PEG as capping agents. The structure and phase composition of the as-prepared UCNPs were detected by XRD. Fig. 1d showed that eight characteristic diffraction peaks of the as-prepared UCNPs were not in conformity with standard XRD patterns of all the known phases of $BaLuF_5$ including monoclinic phase (JCPDS 43-0933, Fig. 1b) and orthorhombic phase (JCPDS 43-0934, Fig. 1a). It's interesting to find that the diffraction peaks of the samples are matched well with the standard cubic phase of $BaGdF_5$ (JCPDS 24-0098). The findings reveal that the as-prepared $BaLuF_5$ UCNPs possess face-centered cubic (FCC) phase structure similar with $BaGdF_5$ host. The $BaLuF_5$ UCNPs undoped with Gd^{3+} possess cubic and monoclinic phase (Fig. 1e), indicating Gd^{3+} doping can favor the phase transformation from monoclinic to cubic. These findings was matched well with previous Liu's and our report for $NaLnF_4$ host.[55,56] The lattice constant of the samples with 30% Gd was calculated to be 5.861 Å. Moreover, no other impurity diffraction peaks were observed, indicating that all of the doping ions were successfully incorporated into the host materials. Furthermore, TEM characterizations were performed to reveal the size and morphology of the as-synthesized $BaLuF_5$:Gd/Yb/Er UCNPs. The typical TEM images in Fig. 2a show that the as-prepared UCNPs were dispersed well. The size distribution of the as-prepared UCNPs (the inset of Fig. 2a) showed that the average size was about 23.7±2.7 nm. The corresponding selected area electron diffraction (SAED) pattern (Fig. 2b) proved that the as-prepared UCNPs had a FCC structure, which was consistent with the above XRD analysis. Fig. 2c showed the typical high-solution TEM (HRTEM) image of a single particle with a measured d-spacing of 3.387 Å, which corresponded to the (111) lattice plane of the cubic phase $BaLuF_5$. Energy-dispersive X-ray spectrometer (EDS) analysis (Fig. 2d) further demonstrated the as-prepared UCNPs containing all the elements: Ba, Lu, F, and the doped Gd, Yb and Er.

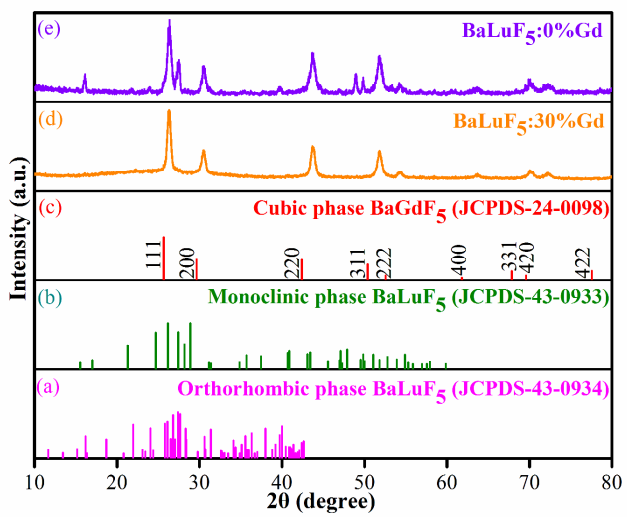

Fig. 1 (a) the standard XRD pattern of orthorhombic phase $BaLuF_5$ (JCPDS 43-0934); (b) the standard XRD pattern of monoclinic phase $BaLuF_5$ (JCPDS 43-0933); (c) the standard cubic XRD pattern of $BaGdF_5$ (JCPDS 24-0098); (d) XRD pattern of the PEG-modified $BaLuF_5$:Gd/Yb/Er UCNPs; (e) XRD pattern of the PEG-modified $BaLuF_5$:Yb/Er UCNPs.

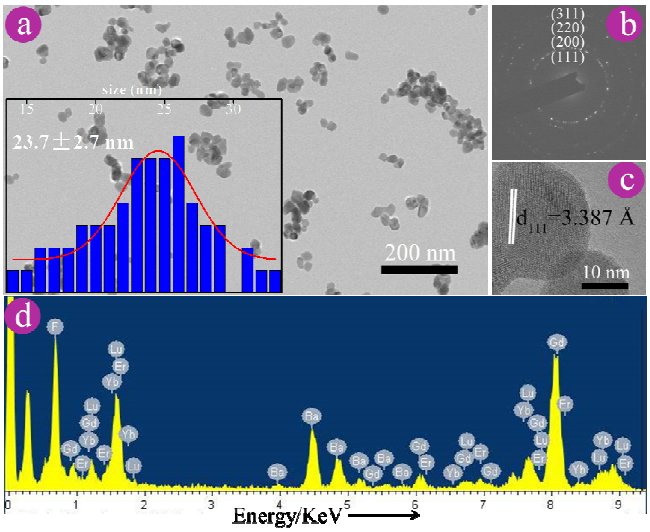

Fig. 2 (a) Typical TEM images of the PEG-modified $BaLuF_5$:Gd/Yb/Er UCNPs; (b) the corresponding SAED pattern; (c) HRTEM image of an individual particle, and (d) EDS pattern. The inset of (a) indicates the size distribution of the particles.

3.2 UC luminescent properties

The UC luminescent spectra of the PEG-modified $BaLuF_5$:Gd/Yb/Er UCNPs were measured by a spectrophotometer under the excitation of 980 nm laser diode. As is shown in Fig. 3a, there were three typical UC emission bands centered at 520/545 (green) and 664 (red) nm, which can be attributed to the electronic transition of $^2H_{11/2}/^4S_{3/2} \rightarrow {}^4I_{15/2}$ and $^4F_{9/2} \rightarrow {}^4I_{15/2}$ of Er^{3+} ions based on the energy level diagram (Fig. S1), respectively. Generally, the UC luminescent intensity (I_{UC}) is proportional to the near-infrared excitation (I_{NIR}), which can be described as the following formula: $I_{UC} \propto I_{NIR}^{n}$. Where n is the number of photon absorbed for each UC emission process. The value of n is determined by the slope of the fitted line in the plot of log I_{UC} versus log I_{NIR}. Fig. 3b revealed that the slopes for the green and red UC emissions of Er^{3+} at 520, 545, and 664 nm are 1.51, 1.81 and 1.64, respectively, indicating that two photons were needed for the green and red emissions.

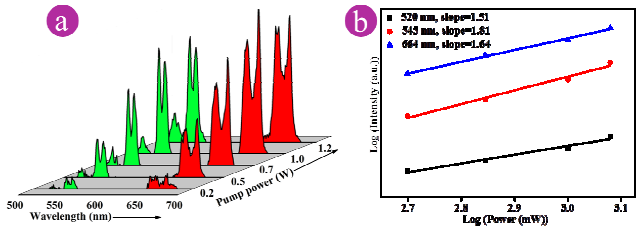

Fig. 3 (a) Upconversion spectrum of the PEG-modified $BaLuF_5$:Gd/Yb/Er UCNPs, (b) the log plots of UC emission intensity verses the laser power.

3.3 *In vitro* cell bioimaging

The PEG modified $BaLuF_5$:Gd/Yb/Er UCNPs can be well dispersed in water as well as can be further conjugated with some special biomolecules for many amine groups, which is suitable for the applications in biology. Therefore, HeLa cells were incubated with the PEG modified $BaLuF_5$ UCNPs for 4 h at 37 ℃ and 5% CO_2 to study the UC optical bioimaging. Fig. 4 showed the *in vitro* cell bioimaging detected by a confocal laser scanning microscopy (ZEISS LSM-710 NLO) under 980 nm excitation. As shown in Fig. 4b and 4c, two intense UC emission channels including green (500-600 nm) and red (700 nm) were respectively detected on the surface of HeLa cells, indicating the as-prepared samples were successfully internalized into the cells. The overlay image (Fig. 4d) showed the UC signals were matched well with HeLa cells. Moreover, the localized luminescence spectra taken from cells and background (inset of Fig. 4d) under the excitation of 980 nm laser revealed the similar luminescent spectra with Fig. 3a and absence of any autofluorescence, further verifying the cell uptake of these UCNPs. All these results demonstrated the $BaLuF_5$ UCNPs can be used as ideal nanoprobes for UC luminescent bioimaging without autofluorescence.

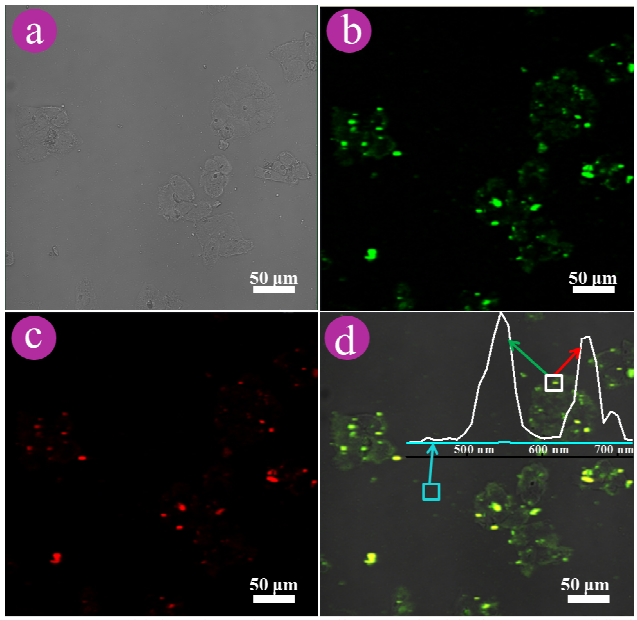

Fig. 4 *In vitro* bioimaging of HeLa cells treated with the PEG modified $BaLuF_5$ UCNPs under 980 nm excitation: (a) bright field image; (b) and (c) the corresponding green (500-600 nm) and red (600-700 nm) luminescent images, respectively; (d) the overlay image. The inset of Fig. 4d shows the corresponding localized spectra taken from HeLa cells and background in the spectral range of 500 to 700 nm with a 980 nm excitation.

3.4 X-ray bioimaging

Except the UC bioimaging, the as-prepared $BaLuF_5$ UCNPs can be also used as X-ray bioimaging agent owing to the large X-ray absorption coefficient of Ba, Lu, Gd and Yb. To reveal the ability of *in vivo* X-ray bioimaging based on these UCNPs, a nude mouse without and with subcutaneous injection of UCNPs was imaged by the above imaging system under X-ray excitation. As demonstrated in Fig. 5b, an obvious X-ray absorption contrast (indicated by red circle) was observed after the injection of these UCNPs, whereas no X-ray signal was observed before injecting the UCNPs (Fig. 5a). These results indicated that these UCNPs can be successfully used as X-ray bioimaging agent.

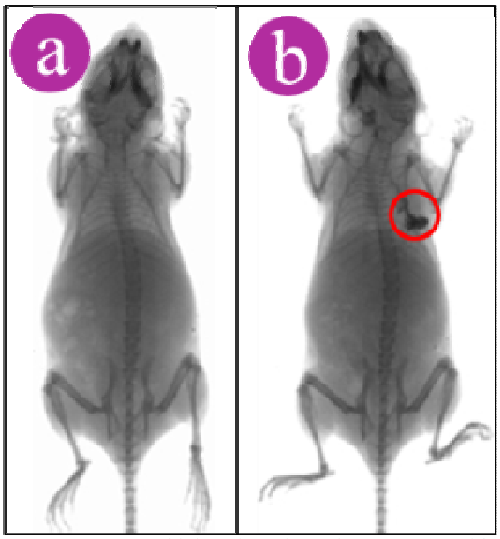

Fig. 5 *In vivo* X-ray bioimaging of a nude mouse: (a) without injection of UCNPs, (b) after the subcutaneous injection of UCNPs.

3.5 Synergistic X-ray and UC bioimaging

To further investigate the synergistic effect of X-ray and UC bioimaging, the simultaneous X-ray and UC bioimaging of a nude mouse was tested by a multi-modal *in vivo* imaging system equipped with an external 980 nm laser as the excitation source and X-ray imaging facility. Fig. 6 shows the *in vivo* bioimaging of a nude mouse without and with subcutaneous injection of the PEG-modified $BaLuF_5$:Gd/Yb/Er UCNPs. As shown in Fig. 6b, an intense UC signal was observed after the injection, while there were no UC signals before injecting the UCNPs (Fig. 6a). The overlay image showed a perfect match of white light and UC emission bioimaging. This result indicated that the as-prepared samples were excellent bioprobes for *in vivo* UC bioimaging. Moreover, the UC and the X-ray signals were matched very well (the right panel of Fig. 6d), indicating the as-prepared UCNPs can be successfully used as dual-modal bioprobes. Furthermore, 30% Gd^{3+} ions in the UCNPs may make it have good paramagnetism and the as-prepared samples may have potential application MRI as ideal contrast agent, suggesting the $BaLuF_5$ UCNPs can be multi-modal bioprobes.

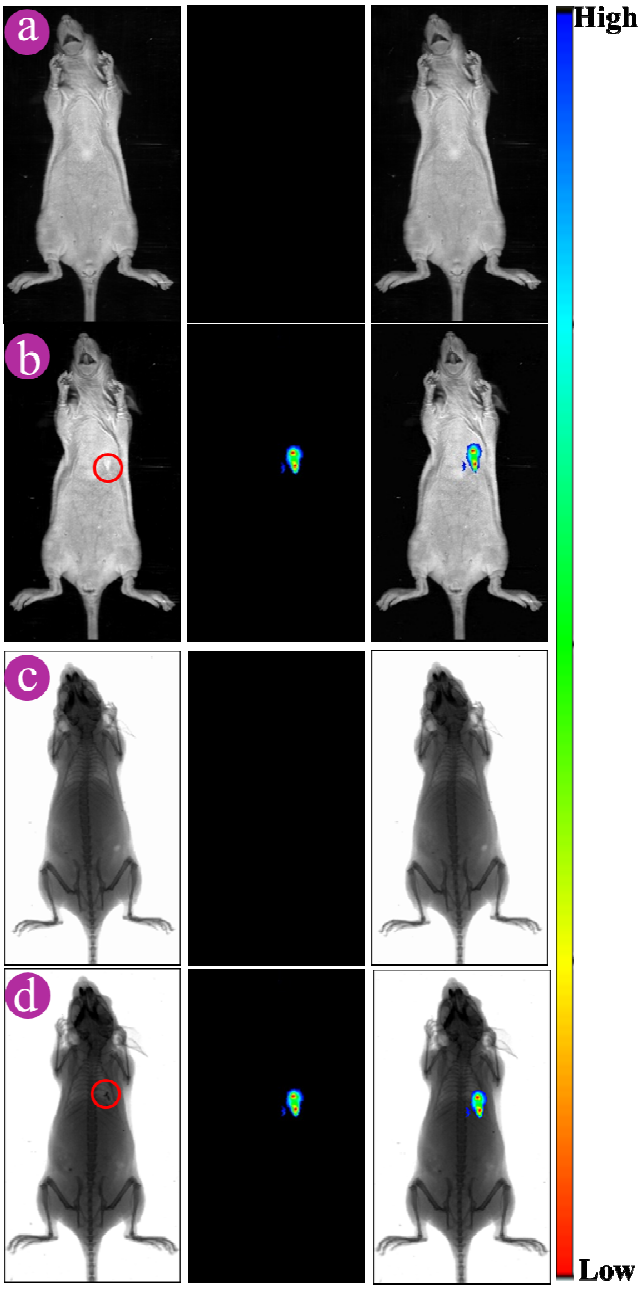

Fig. 6 (a) *In vivo* upconversion luminescent bioimaging of a nude mouse without injection of the $BaLuF_5$ UCNPs: the left panel was white light imaging, the middle panel was UC emission imaging, the right panel was the overlay images; (b) the corresponding imagings after the injection; (c) *In vivo* dual-modal X-ray and UC bioimaging of a nude mouse without subcutaneous injection of UCNPs: the left panel was X-ray imaging, the middle panel was UC imaging, and the right panel was the overlay images; (d) the corresponding images after the injection.

4. Conclusions

A new kind of PEG-modified $BaLuF_5$:Gd/Yb/Er multi-modal bioprobes for UC fluorescent and X-ray bioimaging were synthesized successfully by a one-pot hydrothermal method using PEG as capping ligand. The XRD and TEM results revealed that the as-prepared $BaLuF_5$:Gd/Yb/Er UCNPs presented FCC structure with an average size of 23.7 nm and lattice constant of 5.861 Å. The localized spectra and in vitro cell imaging revealed that intense green and red UC emissions with no auto-

fluorescence centered at 545 and 664 nm were observed from the surface of HeLa cells. In addition, intense UC and X-ray signals were observed in *in vivo* UC and X-ray bioimaging. The perfect matching of UC/X-ray imaging signals verified that the UCNPs can be used as ideal multi-modal bioprobes for synergistically biomedical imaging.

Acknowledgements

This work was supported by the National Natural Science Foundation of China (No. 51102202), specialized research Fund for the Doctoral Program of Higher Education of China (No. 20114301120006) and Hunan Provincial Natural Science Foundation of China (No. 12JJ4056), and Scientific Research Fund of Hunan Provincial Education Department (13B062).

Notes and references

[a] *College of Physics and Information Science and Key Laboratory of Low-dimensional Quantum Structures and Quantum Control of the Ministry of Education, Hunan Normal University, Changsha, Hunan, China. Email: songjunz@hunnu.edu.cn*

[b] *Faculty of Materials, Optoelectronics and Physics, Key Laboratory of Low-dimensional Materials and Application Technology (Ministry of Education), Xiangtan University, Xiangtan 411105, People's Republic of China.*

[c] *Department of Applied Physics and Materials Research Center, The Hong Kong Polytechnic University, Hong Kong.*

1 M. M. Shang, C. X. Li and J. Lin, *Chem. Soc. Rev.*, 2014, **43**, 1372.
2 M. Haase and H. Schäfer, *Angew. Chem. Int. Ed.*, 2011, **50**, 5808.
3 S. J. Zeng, Z. G. Yi, W. Lu, C. Qian, H. B. Wang, L. Rao, T. M. Zeng, H. R. Liu, H. J. Liu, B. Fei and J. H. Hao, *Adv. Funct. Mater.*, 2014, **24**, 4051.
4 F. Auzel, *Chem. Rev.*, 2004, **104**, 139.
5 G. F. Wang, Q. Peng and Y. D. Li, *Acc. Chem. Res.*, 2011, **44**, 322.
6 P. Y. Yuan, Y. H. Lee, M. K. Gnanasammandhan, Z. P. Guan, Y. Zhang and Q. H. Xu, *Nanoscale*, 2012, **4**, 5132.
7 Q. F. Xiao, X. P. Zheng, W. B. Bu, W. Q. Ge, S. J. Zhang, F. Chen, H. Y. Xing, Q. G. Ren, W. P. Fan, K. L. Zhao, Y. Q. Hua and J. L. Shi, *J. Am. Chem. Soc.*, 2013, **135**, 13041.
8 S. J. Zeng, H. B. Wang, W. Lu, Z. G. Yi, L. Rao, H. R. Liu and J. H. Hao, *Biomaterials*, 2014, **35**, 2934.
9 M. Wang, C. C. Mi, W. X. Wang, C. H. Liu, Y. F. Wu, Z. R. Xu, C. B. Mao and S. K. Xu, *ACS Nano*, 2009, **3**, 1580.
10 N. Bogdan, E. M. Rodríguez, F. Sanz-Rodríguez, M. C. I. de la Cruz, Á. Juarranz, D. Jaque, J. G. Solé and J. A. Capobianco, *Nanoscale*, 2012, **4**, 3647.
11 F. C. J. M. van Veggel, C. H. Dong, N. J. J. Johnson and J. Pichaandi, *Nanoscale*, 2012, **4**, 7309.
12 Y. F. Wang, G. Y. Liu, L. D. Sun, J. W. Xiao, J. C. Zhou and C. H. Yan, *ACS Nano*, 2013, **7**, 7200.
13 N. M. Idris, M. K. Gnanasammandhan, J. Zhang, P. C. Ho, R. Mahendran and Y. Zhang, *Nature medcine*, 2012, **18**, 1580.
14 L. He, L. Z. Feng, L. Cheng, Y. M. Liu, Z. W. Li, R. Peng, Y. G. Li, L. Guo and Z. Liu, *ACS Appl. Mater. Interfaces*, 2013, **5**, 10381.
15 P. Huang, W. Zheng, S. Y. Zhou, D. T. Tu, Z. Chen, H. M. Zhu, R. F. Li, E. Ma, M. D. Huang and X. Y. Chen, *Angew. Chem. Int. Ed.*, 2014, **53**, 1252.
16 D. M. Yang, X. J. Kang, M. M. Shang, G. G. Li, C. Peng, C. X. Li and J. Lin, *Nanoscale*, 2011, **3**, 2589.
17 J. Shen, G. Y. Chen, T. Y. Ohulchanskyy, S. J. Kesseli, S. Buchholz, Z. P. Li, P. N. Prasad and G. Han, *Small*, 2013, **9**, 3213.
18 C. Y. Liu, Z. Y. Gao, J. F. Zeng, Y. Hou, F. Fang, Y. L. Li, R. R. Qiao, L. Shen, H. Lei, W. S. Yang and M. Y. Gao, *ACS Nano*, 2013, **7**, 7227.
19 J. H. Hao, Y. Zhang and X. H. Wei, *Angew. Chem. Int. Ed.*, 2011, **50**, 6876.
20 L. Cheng, C. Wang, X. X. Ma, Q. L. Wang, Y. Cheng, H. Wang, Y. G. Li and Z. Liu, *Adv. Funct. Mater.*, 2013, **23**, 272.
21 P. Huang, J. Lin, X. S. Wang, Z. Wang, C. L. Zhang, M. He, K. Wang, F. Chen, Z. M. Li, G. X. Shen, D. X. Cui and X. Y. Chen, *Adv. Mater.*, 2012, **24**, 5104.
22 X. F. Qiao, J. C. Zhou, J. W. Xiao, Y. F. Wang, L. D. Sun and C. H. Yan, *Nanoscale*, 2012, **4**, 4611.
23 B. B. Xu, J. H. Hao, Q. B. Guo, J. C. Wang, G. X. Bai, B. Fei, S. F. Zhou and J. R. Qiu, *J. Mater. Chem. C*, 2014, **2**, 2482.
24 M. He, P. Huang, C. L. Zhang, H. Y. Hu, C. C. Bao, G. Gao, R. He and D. X. Cui, *Adv. Funct. Mater.*, 2011, **21**, 4470.
25 W. Wei, T. C. He, X. Teng, S. X. Wu, L. Ma, H. Zhang, J. Ma, Y. H. Yang, H. Y. Chen, Y. Han, H. D. Sun and L. Huang, *Small*, 2012, **8**, 2271.
26 J. W. Stouwdam and F. C. J. M. van Veggel, *Nano Letters*, 2002, **2**, 733.
27 X. F. Yu, M. Li, M. Y. Xie, L. D. Chen, Y. Li and Q. Q. Wang, *Nano Research*, 2010, **3**, 51.
28 K. W. Krämer, D. Biner, G. Frei, H. U. Güdel, M. P. Hehlen and S. R. Lüthi, *Chem. Mater.*, 2004, **16**, 1244.
29 J. Wang, F. Wang, C. Wang, Z. Liu and X. G. Liu, *Angew. Chem. Int. Ed.*, 2011, **50**, 10369.
30 J. Zhou, Z. Liu and F. Y. Li, *Chem. Soc. Rev.*, 2012, **41**, 1323.
31 Y. S. Liu, D. T. Tu, H. M. Zhu and X. Y. Chen, *Chem. Soc. Rev.*, 2013, **42**, 6924.
32 Q. Liu, Y. Sun, T. S. Yang, W. Feng, C. G. Li and F. Y. Li, *J. Am. Chem. Soc.*, 2011, **133**, 17122.
33 S. J. Zeng, M. K. Tsang, C. F. Chan, K. L. Wong and J. H. Hao, *Biomaterials*, 2012, **33**, 9232.
34 L. Cheng, K. Yang, Y. G. Li, J. H. Chen, C. Wang, M. W. Shao, S. T. Lee and Z. Liu, *Angew. Chem. Int. Ed.*, 2011, **123**, 7523.
35 S. W. Wu, G. Han, D. J. Milliron, S. Aloni, S. Altoe, D. V. Talapin, B. E. Cohen and P. J. Schuck, *Proc. Natl. Acad. Sci. U. S. A.*, 2009, **106**, 10917.
36 R. Naccache, P. Chevallier, J. Lagueux, Y. Gossuin, S. Laurent, L. V. Elst, C. Chilian, J. A. Capobianco and M. A. Fortin, *Adv. Healthcare Mater.*, 2013, **2**, 1477.
37 H. Y. Xing, S. J. Zhang, W. B. Bu, X. P. Zheng, L. J. Wang, Q. F. Xiao, D. L. Ni, J. M. Zhang, L. P. Zhou, W. J. Peng, K. L. Zhao, Y. Q. Hua and J. L. Shi, *Adv. Mater.*, 2014, DOI: 10.1002/adma.201305222.
38 G. Y. Chen, T. Y. Ohulchanskyy, R. Kumar, H. Ågren and P. N. Prasad, *ACS Nano*, 2010, **4**, 3163.
39 C. H. Dong, A. Korinek, B. Blasiak, B. Tomanek and F. C. J. M. van Veggel, *Chem. Mater.*, 2012, **24**, 1297.
40 Y. L. Dai, H. H. Xiao, J. H. Liu, Q. H. Yuan, P. A. Ma, D. M. Yang, C. X. Li, Z. Y. Cheng, Z. Y. Hou, P. P. Yang and J. Lin, *J. Am. Chem. Soc.*, 2013, **135**, 18920.
41 R. Komban, J. P. Klare, B. Voss, J. Nordmann, H. J. Steinhoff and M. Haase, *Angew. Chem. Int. Ed.*, 2012, **51**, 6506.
42 Y. X. Liu, D. S. Wang, J. X. Shi, Q. Peng and Y. D. Li, *Angew. Chem. Int. Ed.*, 2013, **52**, 4366.
43 G. C. Jiang, J. Pichaandi, N. J. J. Johnson, R. D. Burke and F. C. J. M. van Veggel, *Langmuir*, 2012, **28**, 3239.
44 X. S. Zhai, S. S. Liu, X. Y. Liu, F. Wang, D. M. Zhang, G. S. Qin and W. P. Qin, *J. Mater. Chem. C*, 2013, **1**, 1525.
45 H. L. Qiu, G. Y. Chen, L. Sun, S. W. Hao, G. Han and C. H. Yang, *J. Mater. Chem.*, 2011, **21**, 17202.
46 http://physics.nest.gov./PhysRefData/XrayMassCoef/.
47 Y. L. Liu, K. L. Ai, J. H. Liu, Q. H. Yuan, Y. Y. He and L. H. Lu, *Angew. Chem. Int. Ed.*, 2012, **51**, 1437.
48 S. B. Yu and A. D. Watson, *Chem. Rev.*, 1999, **99**, 2353.
49 G. Gao, C. L. Zhang, Z. J. Zhou, X. Zhang, J. B. Ma, C. Li, W. L. Jin and D. X. Cui, *Nanoscale*, 2013, **5**, 351.
50 Y. L. Liu, K. L. Ai, J. H. Liu, Q. H. Yuan, Y. Y. He and L. H. Lu, *Adv. Healthcare Mater.*, 2012, **1**, 461.
51 H. R. Liu, W. Lu, H. B. Wang, L. Rao, Z. G. Yi, S. J. Zeng and J. H. Hao, *Nanoscale*, 2013, **5**, 6023.

52 D. M. Yang, C. X. Li, G. G. Li, M. M. Shang, X. J. Kang and J. Lin, *J. Mater. Chem.*, 2011, **21**, 5923.
53 S. J. Zeng, M. K. Tsang, C. F. Chan, K. L. Wong, B. Fei and J. H. Hao, *Nanoscale*, 2012, **4**, 5118.
54 S. Sarkar, B. Meesaragandla, C. Hazra and V. Mahalingam, *Adv. Mater.*, 2013, **25**, 856.
55 F. Wang, Y. Han, C. S. Lim, Y. H. Lu, J. Wang, J. Xu, H. Y. Chen, C. Zhang, M. H. Hong and X. G. Liu, *Nature*, 2010, **463**, 1061.
56 S. J. Zeng, J. J. Xiao, Q. B. Yang and J. H. Hao, *J. Mater. Chem.*, 2012, **22**, 9870.

One-pot synthesis of PEG modified $BaLuF_5$: Gd/Yb/Er nanoprobes for dual-modal *in vivo* upconversion luminescent and X-ray bioimaging

Ling Rao,[a,b] Wei Lu,[c] Tianmei Zeng,[a] Zhigao Yi, [a,b] Haibo Wang, [a,b] Hongrong Liu[a] and Songjun Zeng[*a]

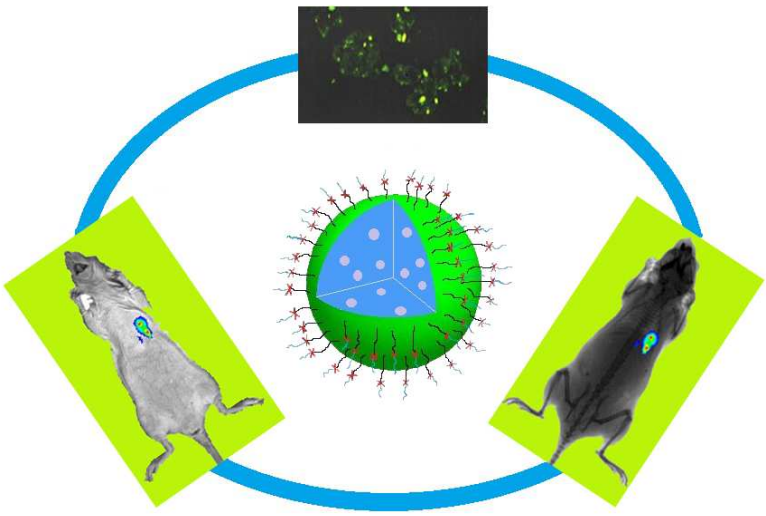

PEG-modified $BaLuF_5$:Gd/Yb/Er nanoparticels synthesized by hydrothermal method for *in vivo* and in vitro bioimaging and X-ray bioimaging.